

Cornell University Unmanned Air Systems

2018 AUVSI SUAS Competition

Theia II Technical Design



Abstract

Cornell University Unmanned Air Systems (CUAir) designed a modular system capable of being manufactured, tested, and rebuilt in parallel to participate in the 2018 AUVSI SUAS competition. Using data and past experience, the team endeavored to perfect CUAir's previous Unmanned Aerial System (UAS), Theia, by creating an improved system, Theia II, with unmatched flight performance and efficiency. Theia II was the result of the joint effort of 50 undergraduate students from the fields of Computer Science, Electrical Engineering, Mechanical & Aerospace Engineering, Mathematics, and Physics. By combining knowledge from these fields, the team constructed a custom airframe with modular parts, a robust power system, a well-tuned autopilot, a fully modular distributed imagery system, and a custom ground control station. Throughout the year, CUAir rigorously tested the system to ensure the reliability of every component.



1. Systems Engineering Approach

The Theia II system was designed, manufactured, and tested to perform an autonomous search and rescue mission at the AUVSI SUAS competition as safely, reliably, and accurately as possible. The system is capable of autonomous flight, obstacle avoidance, image surveillance, autonomous and manual object detection, and air delivery. The following sections describe the mission tasks, identify requirements for successful mission execution, and justify the resulting system design decisions implemented to fulfill these requirements.

1.1. Mission Requirement Analysis

The mission demonstration simulates a forest fire search and rescue operation. Each team receives mission details and deploys the UAS, which flies to the object area, locates the forest fire and the person of interest, and suppresses the fire using water.

Table 1 describes the goals of each mission task and the requirements CUAir and the UAS must achieve to reach each goal. The requirements of the Autonomous Flight and Obstacle Avoidance tasks call for an aircraft that is acrobatic enough to enable the autopilot to precisely navigate to all waypoints and to steer clear of moving obstacles. The Object Detection, Classification and Localization task requires a high resolution camera

Task	Description	Successful Mission Execution Requirements
Timeline (10%)	<ul style="list-style-type: none"> Complete the mission in minimal flight and post-processing time (80%) Refrain from taking a timeout (20%) 	<ul style="list-style-type: none"> Well practiced full mission tests Completion of the mission as quickly and safely as possible
Autonomous Flight (30%)	<ul style="list-style-type: none"> Fly autonomously with minimal manual takeovers (40%) Fly a waypoint sequence within 100 ft of each waypoint (10%) Hit waypoints in a sequence as accurately as possible (50%) 	<ul style="list-style-type: none"> A fully functioning autopilot capable of path execution, autonomous takeoff, and autonomous landing An agile airframe that can be easily manoeuvred to hit waypoints and maximize $\max(0, \frac{150 \text{ ft} - \text{distance}}{150 \text{ ft}})$
Obstacle Avoidance (20%)	<ul style="list-style-type: none"> Avoid stationary obstacles, i.e. cylinders with radius 30ft to 300ft and height 30ft to 750ft (50%) Avoid moving obstacles, i.e. spheres with radius 30ft to 300 ft moving between 0 KIAS and 40 KIAS (50%) 	<ul style="list-style-type: none"> An algorithm adept at predicting obstacle locations and recalculating flight paths An autopilot system that is able to relay telemetry data to interoperability server at rate of 1Hz
Object Detection, Classification, Localization (20%)	<ul style="list-style-type: none"> Identify object shape, shape color, alphanumeric, alphanumeric color, and orientation (20%) Identify the GPS location of each object (30%) Submit objects during the first flight via the Interoperability System (30%) Provide the above information autonomously (20%) 	<ul style="list-style-type: none"> A system capable of manual detection and classification of objects and object submission A system capable of autonomous detection and classification of objects and object submission A mechanically stable imaging system and high resolution camera An algorithm that can use telemetry metadata to accurately compute the location of each object
Air Delivery (10%)	<ul style="list-style-type: none"> Navigate to drop location and deliver 8 oz water bottle, dispersing the water on impact Do not drop outside of given location to avoid Things Falling Off Aircraft Penalty 	<ul style="list-style-type: none"> A mechanism that is able to drop a bottle reliably and to ensure the bottle opens on landing An algorithm that can calculate the optimal release time to maximize $\max(0, \frac{150 \text{ ft} - \text{distance}}{150 \text{ ft}})$
Operational Excellence (10%)	<ul style="list-style-type: none"> Exercise operational professionalism, communication between members, reaction to system failures, and attention to safety 	<ul style="list-style-type: none"> Gracious professionalism and practice with clear communication and alertness from all team members

Table 1: Mission Requirement Analysis

capable of capturing images of sufficient resolution to identify objects while imaging the entire search area. The task also requires stabilization of the camera, a high-speed data link, and a server to process images. When designing the aircraft, the team must consider the trade-off between acrobatic performance for the Autonomous Flight and Obstacle Avoidance tasks and greater stability for the Object Detection, Classification, and Localization task. Air Delivery requires a mechanism capable of reliably dropping the water bottle and a system to optimally time the release. Timeline and Operational Excellence require full mission tests to ensure all systems function reliably and all personnel are trained.

CUAir chose to use the previous year's system as a starting place for the 2018 system. To improve performance on Autonomous Flight, the team needed to build a better navigation algorithm to hit waypoints more accurately. To ensure the system avoids all obstacles, the team needed to create a software system that incorporates input from a human operator. To guarantee all object characteristics are discernible, the team needed to integrate a high resolution camera. To maximize safety and accuracy for Air Delivery, the team needed to build a mechanically consistent system with minimal points of failure.

1.2. Design Rationale

The Theia II system was designed to maximize mission performance. The team identified the importance of each task and made decisions accordingly within the team's qualifications and budget. **Figure 1** shows the flow of design decisions.

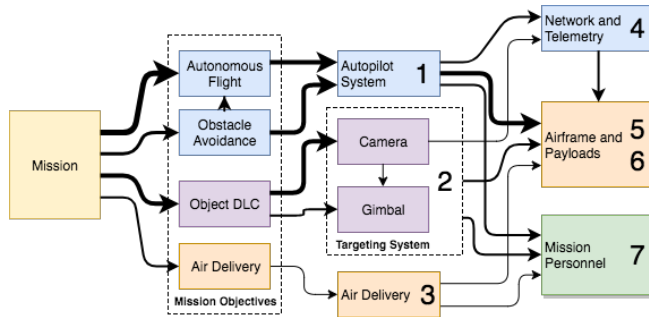


Figure 1: Flow of design decisions, thicker lines indicate a higher priority dependency.

The first design decision was the choice of navigation system due to its importance in achieving mission tasks, primarily in Autonomous Flight and Obstacle Avoidance. The 3DRobotics Pixhawk autopilot was chosen for its customizability, large support community, and familiarity to the team. The Pixhawk provides accurate and reliable autonomous navigation capabilities. The autopilot's open source nature also enables the team to

write custom firmware to improve Waypoint Accuracy.

The second decision was the choice of an imaging system. The team chose the uEye LE industrial camera with an 8 mm lens due to its ability to capture images of objects of sufficient resolution and quality in turbulent flying conditions. The team decided a gimbal was necessary to control the camera for the point-at-ground and off-axis object capabilities needed to accomplish the Object Detection, Classification, Localization task. Overall, the imagery system chosen exceeds the capabilities deemed necessary in **Section 2.4** and is within the team's budget.

The third decision was the design of the air delivery system. The team designed a robust and consistent mechanism using a linear actuator to drop the bottle. The mechanism is located near the aircraft's center of gravity so that the release of the bottle does not affect stability during flight.

The fourth decision was the choice of network and telemetry systems to enable Actionable Intelligence and Object Detection, Classification, Localization in flight. To fulfill the networking requirements of the autopilot and the camera, wireless data protocols and antennae were chosen to enable fast and accurate data transmission between the aircraft and the ground station. These links are established with a Ubiquiti Rocket-AC pair for WiFi and RFD900+ radio pair for telemetry.

The fifth decision was the design of payload controllers. To meet the requirements of the camera, gimbal, communication, airdrop, and autopilot systems, the payload controllers must be able to provide power to all of these components, communicate with the ground station, control the airdrop system, and point the gimbal to assist in the discovery of objects. The team designed custom circuit boards to fit these requirements.

The sixth design decision was airframe design. The aircraft must support a fuselage carrying the camera, gimbal, payloads, airdrop package, and power supply while also meeting the maneuverability requirements of Autonomous Flight and Obstacle Avoidance. The team had to consider trade-offs between agility, accurate waypoint capture, speed for Timeline, and stability for better image quality. To optimize for overall mission success, a large wing surface area was chosen to slow flight, improving waypoint accuracy and image quality. CUAir decided to use a pneumatic catapult and belly-landing instead of traditional landing gear. Pneumatic catapults allow for smooth and consistent take-offs without a clear runway, which was necessary for the team in the often snowy and muddy conditions of Upstate New York.

Lastly, mission personnel were decided. Team members were chosen based on experience operating task-related functions and familiarity with the design.

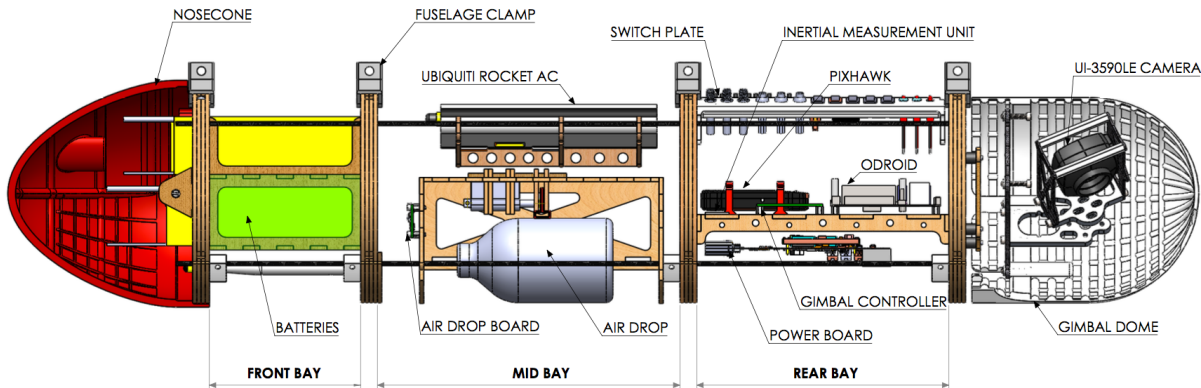


Figure 2: Fuselage Inner Section

2. System Design

2.1. Aircraft

The airframe's success in the 2017 AUVSI SUAS mission validated its design and proved its reliability, so CUAir decided to reuse the Theia airframe in the Theia II UAS. The airframe's modular design allowed the team to quickly perform standard maintenance to replace fatigued and damaged components to keep the airframe in good condition after nearly two years of use. This standard maintenance ensured that the airframe will remain safe and reliable during the 2018 mission.

The airframe was designed around a central boom with detachable wings, tail, and fuselage for easy transportation and modification. This modularity allows fuselage components to be interchanged for test flights and facilitates adjustment of the center of gravity with respect to the wings and tail. The movable fuselage is attached to the boom with adjustable 3D printed clamps and is divided into three bays, as shown in **Figure 2**. Lithium polymer (LiPo) batteries are stored in the front bay and are accessible via the removable nosecone of the aircraft. The airdrop system is in the mid bay, located below the aircraft's center of gravity. The rear bay houses the system's autopilot, on-board computer, and supporting electronics. The camera and gimbal attach to the rear of the fuselage. This divided bay system provides greater modularity and accessibility than a uni-body design. The aircraft weighs 24.9 lb, including payloads. The airframe dimensions are shown in **Figure 4**. Complete specifications and performance data are given in **Table 2**.

The airframe was built to withstand high shock forces associated with catapult assisted take-off and belly landing. The wings and tail are made out of a composite structure of polystyrene foam and balsa wood sheeting with a Garolite and carbon fiber substructure. The wings connect to each other and to the boom with carbon

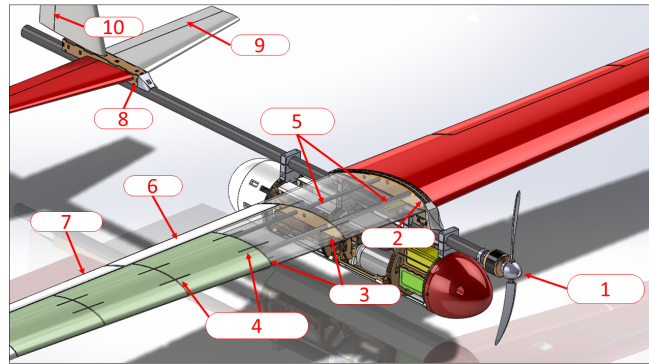


Figure 3: Airframe Design - Monokote and skin transparent to show inner wing components. Labels refer to: (1) AXi 5320/28 Motor, (2) Wing Plate, (3) Plywood Ribs, (4) Carbon Fiber Reinforcements, (5) Carbon Fiber Spars, (6) Right Flap, (7) Right Aileron, (8) Tailbox, (9) Left Elevator, (10) Rudder

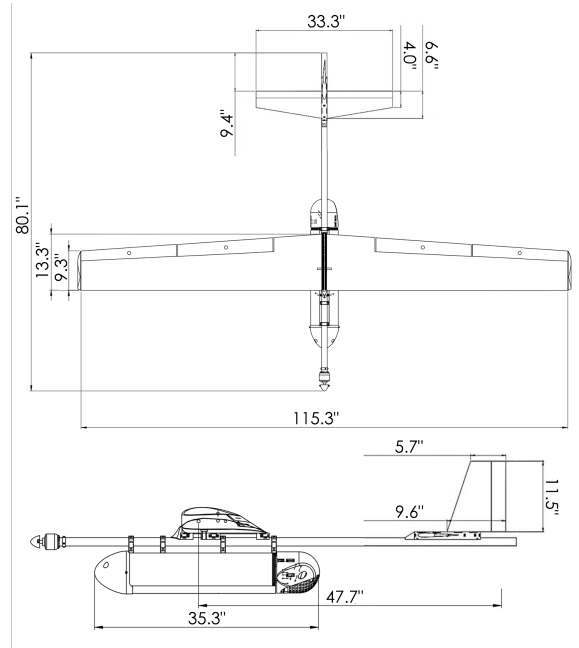


Figure 4: Theia II Aircraft Projections, Dimensions Shown

fiber spars through the wing plate. This connection is shown in **Figure 3**. The fuselage firewalls, wing plate, and tailbox are made out of laser-cut plywood. The nosecone and gimbal dome are made out of 3D-printed ABS plastic.

The flight surfaces of the aircraft were load tested to a factor of safety of 2 times the weight of the aircraft as shown in **Figure 5**. The wing plate was designed for controlled breakage in the event of a crash. This allows the wings to break away from the boom and be salvaged for reuse. A finite element analysis showing the intended weak points is shown in **Figure 6**. When designing the fuselage, each subsection of the modular design was weight-reduced and rigorously tested to ensure structural integrity during simulated impact forces. The attachment mechanism between the boom and the fuselage was tested in both shear and tensile scenarios by applying a constant torque and force, respectively. These tests subjected the mechanism to 2 times the maximum forces expected during take-off, flight, and landing. Attachment mechanism designs with three different 3D printed materials (ABS, PLA, and carbon fiber infused nylon) were tested. The carbon fiber infused nylon was found to have the highest strength-to-weight ratio while still meeting the safety requirements.

An AXi 5320/28 brushless motor, a 120A ESC, and a 9-cell LiPo battery were chosen as the propulsion system to allow for a flight time of 30 minutes at 70% throttle. Using an electric motor instead of an internal combustion engine minimizes vibrations and increases image clarity for the vision system.

The proven reliability of the the airframe design gives CUAir confidence in meeting the requirements identified in **Section 1.1**.



Figure 5: Distributed load test with 50 lbs, 2 times the weight of the aircraft.

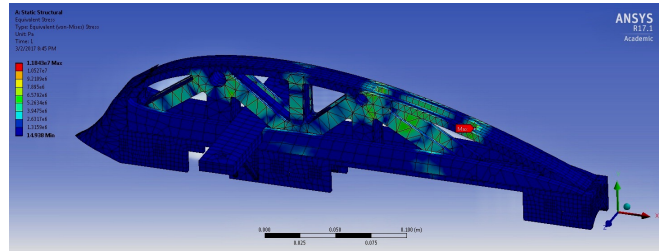


Figure 6: ANSYS model of the wing plate with color-coded stress distribution shown.

	Wing	Vertical Stabilizer	Horizontal Stabilizer	Aircraft Dimensions and Specifications		Performance	
Airfoil	MH-114	Drela HT-12	Drela HT-12	Length (ft)	5.91	Cruise Speed (ft/s)	46
Span (ft)	9.45	.96	2.66	Width (ft)	9.45	Max Speed (ft/s)	82
Area (ft ²)	6.96	.465	.927	Height (ft)	1.54	Min Speed (ft/s)	39
Avg. Incidence Angle (°)	2.00	0.00	-2.18	Weight (lb)	17.4	Min Turn radius (ft)	66
Aspect Ratio	10	1.5	6	Prop. Size (in x in)	17x10	Flight Hours (hrs)	7.5
Lift (lbf)	25.72	0	-.724	Motor	Axi 5320/28	Total Flight Time (min)	30
Mean Aero Chord (ft)	.866	.568	.400	Payload Weight (lb)	7.5	Assembly Time (min)	5

Table 2: Aircraft Specifications and Performance

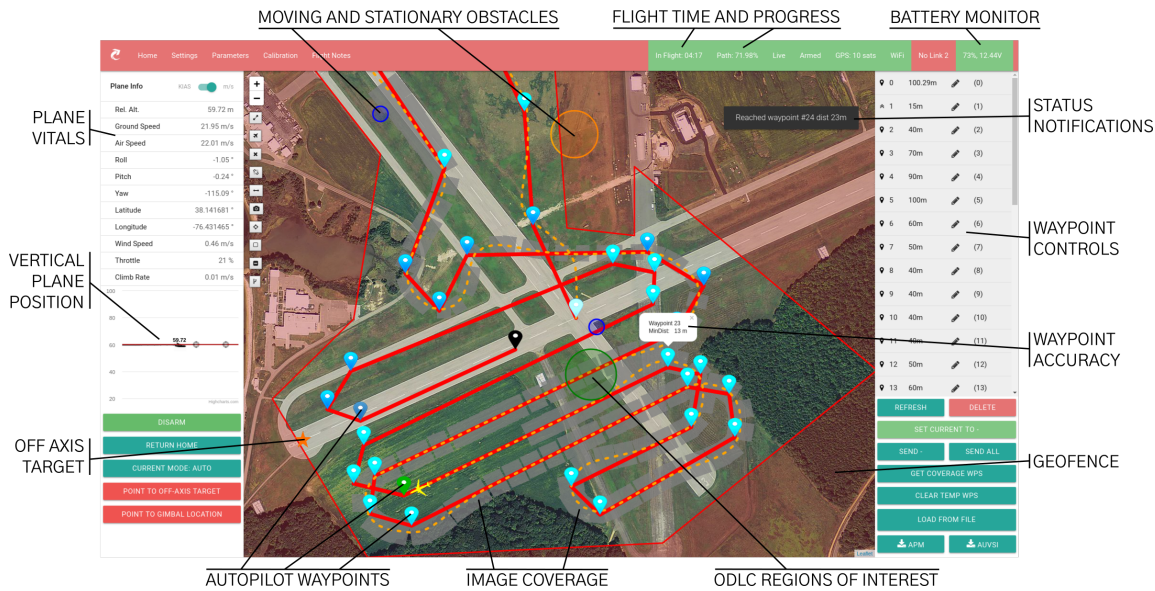


Figure 7: Autopilot GCS

2.2. Autopilot

The Theia II system uses a 3DRobotics Pixhawk along with a full sensor suite for autonomous navigation, diagrammed in **Figure 8**. The Pixhawk has plug-and-play support for common sensors, making it easy and highly affordable to test many systems simultaneously on appropriate platforms before integration into the Theia II system. Thus, the team was able to tune the autopilot for flight while testing obstacle avoidance algorithms on a test airframe, the Bix3, as well as collecting imaging and geolocation data on a hexacopter that was easier to navigate. The Pixhawk autopilot also makes it easier to meet competition safety requirements with numerous features including redundant power, support for redundant telemetry radios, and a hardware safety switch. The full autopilot system diagram is shown in **Figure 10**.

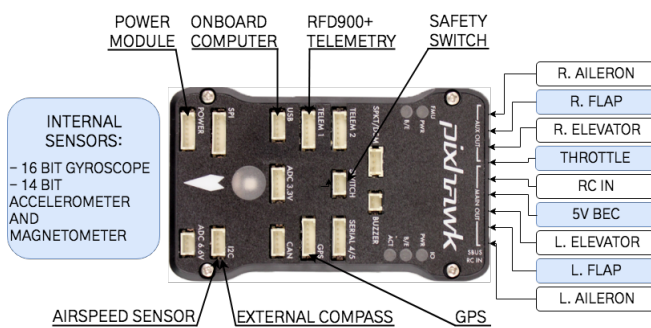


Figure 8: Pixhawk Sensor Diagram

The Pixhawk runs modified ArduPilot 3.8 firmware. ArduPilot was the best choice for the Pixhawk since it is

the most popular open-source firmware currently available, provides developer support, and has many essential flight features required for autonomous flight. ArduPilot is capable of waypoint navigation, autonomous takeoff, and autonomous landing, so the team will not need to incur any pilot takeover penalties.

The system is configured for catapult launch, waiting for an acceleration of 26 ft/s^2 (approximately half of the measured acceleration during a typical launch) before engaging the throttle. This allows for consistent takeoffs without access to a runway. To ensure that the UAS lands safely, the system is able to touch down consistently using only GPS and a properly tuned barometer.

Another important advantage of ArduPilot is that it is open source, meaning the team can customize the autopilot firmware. Two small customizations were implemented: autonomous initialization of flaps prior to takeoff, which provides additional lift at the beginning of the launch; and precise flight termination maneuvers, which allow the system to meet AUVSI flight termination requirements. Additionally, the team developed an improved waypoint path following algorithm in place of the ArduPilot L1 Navigation Controller. The algorithm uses properties of Bézier spline curves to plan smooth curved paths that drastically reduce the curvature of the system's trajectory, allowing the aircraft to take smoother turns and hit waypoints more accurately. This change improved Theia II's average waypoint hit radius from 20 feet to 12 feet. A side by side comparison of the system's path taken using the L1 Controller and using CUAir's spline controller is shown in **Figure 9**.

CUAir developed a custom autopilot Ground Control Station (GCS), shown in **Figure 7**. The custom GCS enables the autopilot operator to meet the AUVSI mission

requirements of connecting to the interoperability server, relaying telemetry data, and displaying obstacles, all without leaving the GCS interface. By combining GCS features like aircraft vitals and waypoint modification into a single interface, the GCS operator is able to optimize for mission objectives more efficiently than with an alternative GCS. For example, the GCS operator can view the aircraft's position relative to both stationary and moving obstacles and determine if it is necessary to modify waypoints. The GCS displays the areas of the search grid that have not been imaged to help the GCS operator ensure the UAS has collected images of every object. Additionally, as the aircraft flies the waypoint path, the GCS indicates the point value achieved for each waypoint, helping the GCS operator determine if the waypoint path must be flown again.

The team evaluated the autopilot system both virtually in software simulations and in the field on a test platform before integration into the Theia II system. The virtual tests required the autopilot to perform in a simulated environment, using simulated autopilot hardware and a flight dynamics model provided by the JSBSim library. The Software in the Loop (SITL) simulation environment provides the ability to rapidly perform many tests without the man-hours required to test on a physical aircraft. Four simulated flights are required to prove that new parameters or small tweaks are ready to move forward in testing.

Once the simulated tests passed all requirements, the feature was integrated into a hardware test platform. The team used a HobbyKing Bix3 airframe, a low cost and easy to fly foam platform. With this hardware, the team tested the actual autopilot hardware and its interfaces to motors and sensors. New parameters or small changes to the system were verified by successfully

completing four test flight across two different days.

A summary of testing completed in the SITL, on the Bix3, and on Theia II is shown in **Table 3**.

Before every flight with the Bix3 or the Theia II system, the team tested all on-board sensors including the gyroscope, accelerometer, airspeed sensor, and GPS to confirm that no damage had occurred during transport or flight.

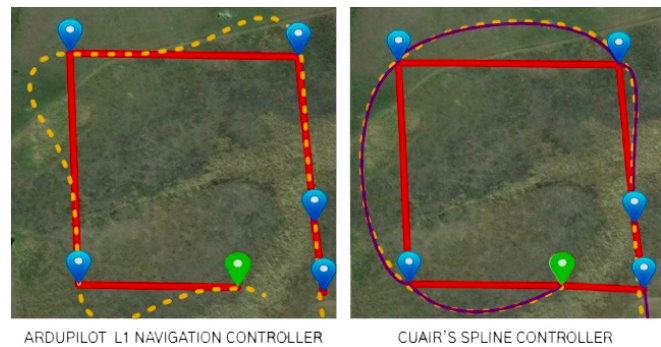


Figure 9: The left image shows the system flying a sequence of waypoints using the default, ArduPilot L1 Controller. The right image shows the system flying the same waypoints using CUAir's improved spline controller.

	SITL	Bix3	Theia II
Total Flight Hours	600	20	8
Total Autonomous Flight Hours	600	15	6
Total # Waypoints Hit	500,000	3,600	2,300
Average Waypoints Miss Distance (ft)	9	10	12

Table 3: Summary of Autopilot Testing

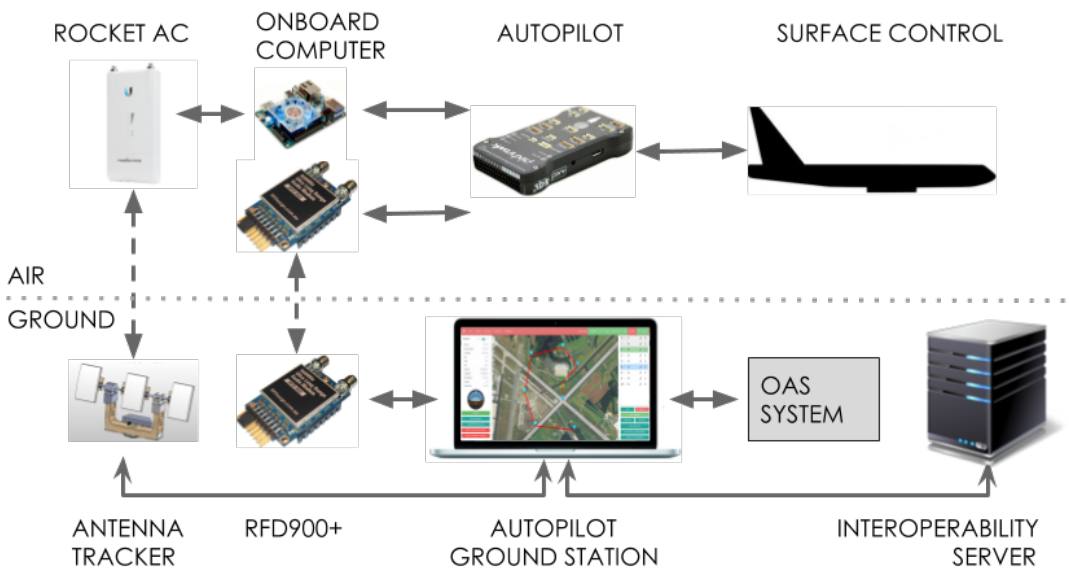


Figure 10: Autopilot Full System

2.3. Obstacle Avoidance

CUAir developed an Obstacle Avoidance System (OAS) for the Obstacle Avoidance task. The task is completed by an OAS Operator on a modified version of the GCS. The decision to use an OAS Operator, as opposed to a fully autonomous system, was motivated by the importance of safety and predictability during the flight, as well as the need to precisely cover the search grid. While an autonomous system has an advantage over a human operator in terms of speed of path rerouting, a human is necessary to account for safety concerns, and to ensure the augmented paths allow for correct execution of the mission requirements.

The operator interacts with the OAS system through an “OAS operator mode” in the GCS. This mode combines waypoint modification tools of the GCS with a visualization of future obstacle and UAS positions generated by the system’s predictive models.

To obtain accurate predictions of moving obstacle locations, the team uses a proprietary online machine learning algorithm, which improves its predictions over time by analyzing obstacle motion. The predictions come in the form of spline curves, which interpolate the previously seen obstacle positions and attempt to predict future obstacle positions. This algorithm is able to provide highly accurate obstacle predictions when provided enough data.

Predicting the future position of the UAS is accomplished by simulating the autopilot’s navigation algorithm in the OAS system and interpolating to construct an accurate approximation of the entire flight path. These data are combined with the predictions of obstacle positions to give the OAS operator accurate data to avoid potential collisions.

Throughout development of the OAS, the team conducted extensive software unit testing to validate correctness and reliability of the system. The team also performed extensive testing with SITL simulation of Theia II to ensure the accuracy and robustness of the obstacle and UAS prediction models, as well as the proper function of the “OAS operator mode” of the GCS. Over 80 hours of testing in the SITL were conducted to

ensure correct functionality of the OAS. This included hitting over 7,500 waypoints and avoiding over 3,000 obstacles. Once the team was confident in the correctness and reliability of the system, over a dozen test flights with the Bix3 system were conducted to determine the system efficacy in a real-world environment. The Bix3 system successfully avoided 63 stationary and 24 moving obstacles. The OAS was then integrated with the Theia II system, on which the team conducted the rest of the flight tests, as shown in **Table 4**.

Total Flight Hours with OAS Active	4
Total # Static Obstacles Tested Against	84
Total # Static Obstacles Avoided	79
Total # Moving Obstacles Tested Against	35
Total # Moving Obstacles Avoided	31

Table 4: Summary of OAS tests in Theia II

2.4. Imaging System

CUAir chose the camera to meet three primary objectives. The first two are maximizing image resolution and fully imaging the search area. These properties ensure both manual and autonomous agents can accurately identify every object and all characteristics for the Object Detection, Classification, and Localization task. The second objective is to support transferring images in flight to achieve Actionable Intelligence. To meet this requirement, the camera must support a simple application program interface (API) that enables remote control of camera functionality and image transfer.

CUAir completed a comprehensive analysis of several cameras. By studying photos taken at previous competitions by the team, it was determined that a minimum resolution of 12 pixels/ft is necessary to resolve object shape and alphanumeric. The required capture rate varied based on flight altitude and sensor/lens configuration. A complete analysis of these metrics is shown in **Table 5**. The team determined that the IDS UI-3590LE (referred to as the uEye) with an 8mm TAMRON M118FM08 lens was the best choice due to its fast frame rate and high object resolution. The uEye additionally supports a well documented API that allows

Camera	Sensor Size (mm)	Lens Focal Length (mm)	Resolution (pixels)	Max Achievable Capture Rate (s/image)	Required Capture Rate (s/image)	Object Resolution (pixels / ft)
ZCAM (2017 Config.)	17.3 x 13	12	4640 x 3480	2.5	4.5	14
ZCAM (New Config.)	17.3 x 13	20	4640 x 3480	2.5	2.7	23
uEye	6.14 x 4.605	8	4912 x 3684	1.5	2.0	33

Table 5: Analysis of several camera configurations



Figure 10: Example image of a green ‘W’ on an orange square captured from 200 feet

control of all camera settings over USB 3.0. The team configured the uEye to use a large aperture, fast shutter speed, and low gain to ensure images had minimal noise and no motion blur.

During flight testing, images were taken at 197 feet. All images were exceptionally clear, and the measured resolution was 33 pixels/ft. An example image of an object is shown in **Figure 10**.

2.4.1. Gimbal

The camera is mounted to a two-axis gimbal system. This configuration allows the camera’s roll and pitch to be controlled independently of the aircraft’s orientation. This allows the plane of the image to be parallel to the ground, which is required by the geolocation algorithm described in **Section 2.5**. Additionally, the gimbal is used to point the camera at off axis objects. The gimbal motors are controlled by a SimpleBGC 32-bit gimbal controller board.

2.5. Object Detection, Classification, Localization

The Imaging Ground Server (IGS) enables manual and autonomous agents to complete the Object Detection, Classification, and Localization (ODCL) task. The IGS interfaces with the on-board computer over the communications network described in **Section 2.6**. Each image is sent to the ground with corresponding telemetry and gimbal metadata and is stored in a database within the IGS. The full ODCL system is diagrammed in **Figure 11**.

The IGS computes the orientation and GPS location of objects given input from the manual and autonomous systems. To find the orientation of the alphanumeric heading, θ_{Obj} , the IGS system computes **Equation 1**.

$$\theta_{\text{Obj}} = (\psi + \theta_{\text{Obj/Img}}) \bmod (360) \quad (1)$$

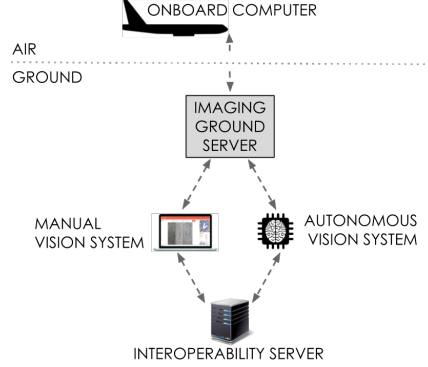


Figure 11: Diagram of the Object Detection, Classification, and Localization system

ψ is the yaw relative to north of the system at the time of image capture and $\theta_{\text{Obj/Img}}$ is the yaw of the objects with respect to the top of the image.

The gimbal points the camera towards the ground for all objects within the geofence. Post-processing of images corrects for image skew from the camera lens and for small errors in the gimbal’s orientation. During testing, the team found that a first order linear transformation was sufficient to remove image skew. The resulting skew corrected image can be scaled by a constant factor to convert from pixels to feet. This simplifies geolocation calculations by effectively removing the aircraft’s roll and pitch. The following algorithm describes the process of geolocating an object identified within a skew-corrected image.

- Orient the image, P , to axis-align it with North and East using aircraft yaw, ψ .

$$P' = \begin{bmatrix} \cos(\psi) & \sin(\psi) \\ -\sin(\psi) & \cos(\psi) \end{bmatrix} P$$

- Find the displacement, D_{xy} , of the objects from the center of the image in pixels.

$$D_{xy} = \begin{bmatrix} O'_x - \frac{W}{2} \\ O'_y - \frac{H}{2} \end{bmatrix}$$

O' is the object location in the rotated image. W and H are the width and height of the image in pixels, respectively.

- Convert the displacement to feet.

$$D_{\text{ft}} = D_{xy} \left[\frac{\frac{2}{W} \times T_{\text{alt}} \tan(\frac{\text{FOV}_h}{2})}{\frac{2}{H} \times T_{\text{alt}} \tan(\frac{\text{FOV}_v}{2})} \right]$$

T_{alt} is the altitude at time of image capture



from telemetry data. FOV_h and FOV_v are the horizontal and vertical fields of view, respectively.

4. Compute the object latitude and longitude using the displacement and image center.

$$O_{\text{lat},\text{lon}} = T_{\text{lat},\text{lon}} + \frac{\text{degrees}}{\text{feet}} \times D_{\text{ft}}$$

$O_{\text{lat},\text{lon}}$ is the object location in degrees latitude, longitude. $T_{\text{lat},\text{lon}}$ is the latitude and longitude of the center of image as determined from the telemetry data at time of image capture. Since the search area is small relative to the size of the Earth, latitude and longitude are assumed to be orthogonal and can be scaled to convert from feet back into degrees.

Testing the geolocation algorithm at test flights demonstrated sufficient accuracy, as shown in **Table 6**. The localization algorithm was tested on different images of the same objects and on objects at both the edges and center of the image. The algorithm for calculating the object's orientation was tested for all eight cardinal and intercardinal orientations. The system consistently localizes the object in the image within 17 ft of the true position.

Number of objects tested	40
Mean error	17 ft
Std. Dev. of error	22 ft
Orientation accuracy	100%

Table 6: Localization System Statistics. Differences in distance were computed by comparing GPS locations calculated by the IGS to GPS locations measured on the ground.

2.5.1. Manual Vision System

The Manual Vision System (MVS) allows for manual detection, localization and classification of objects in images. Once an image is received on the ground, an MVS operator identifies objects within the image, tags characteristics, and marks whether or not the image contains the emergent object. The MVS User Interface (UI) allows the operator to adjust image brightness, saturation, or contrast to improve image clarity. Once an object is tagged on the UI, the IGS system uses associated telemetry and gimbal metadata to compute the orientation and GPS location of the object. An MVS operator can additionally adjust the calculated GPS position by shifting the image to match an underlying

satellite image. Since the tagging procedure is time-consuming and there are many images, the MVS system supports multiple MVS operators simultaneously tagging images across different computers. This allows the team to consistently achieve Actionable Intelligence and minimizes flight time, improving the team's Timeline score.

The IGS and MVS pipeline, from image capture to front-end tagging, was tested extensively with mock data on the ground and real data in the air to discover and resolve any and all software issues.

2.5.2. Autonomous Vision System

Detection and Classification

The Autonomous Vision System (AVS) performs detection and classification of objects for Autonomy. The AVS relies on heuristic and machine learning algorithms to detect and identify objects sightings in images retrieved from the aircraft through the IGS. The system starts by finding regions of interests (ROIs) using the SURF detection algorithm, which has a high recall for blob features similar to objects. ROIs are filtered by several heuristic filters before being fed into a deep learning model to improve target precision rates.

After a ROI is identified as containing a target, a semantic segmentation algorithm (recently published by a group at UC Berkeley¹) gets the contours of the target's shape and alphanumeric. Further algorithms use these contours to classify the target's shape, alphanumeric, orientation, and shape and alpha colors. The shape classification method uses Fourier analysis on the shape contours to retrieve approximate shape descriptors. The shape descriptors are fed into a neural network trained on generated data. The segmented alphanumeric is passed into the Tesseract optical character recognition (OCR) engine. Orientation of the image is reported by the OCR engine as the angle at which the highest confidence for the classified character was recognized. The contours are also used to find the average color of each region. Color classification uses a K-Nearest Neighbors (KNN) model to classify based on several hundred crowd-sourced human identified colors.

False Positive Elimination

False positives are occasionally reported from the classifiers. These objects are noise on the field or a different object altogether. To maximize score, the system attempts to eliminate false positives to avoid extra-object penalties. One way the system avoids false positives is by not reporting any region of interest that

¹Fisher Yu and Vladlen Koltun. "Multi-Scale Context Aggregation by Dilated Convolutions". In: *CoRR* abs/1511.07122 (2015). arXiv: 1511.07122. URL: <http://arxiv.org/abs/1511.07122>.

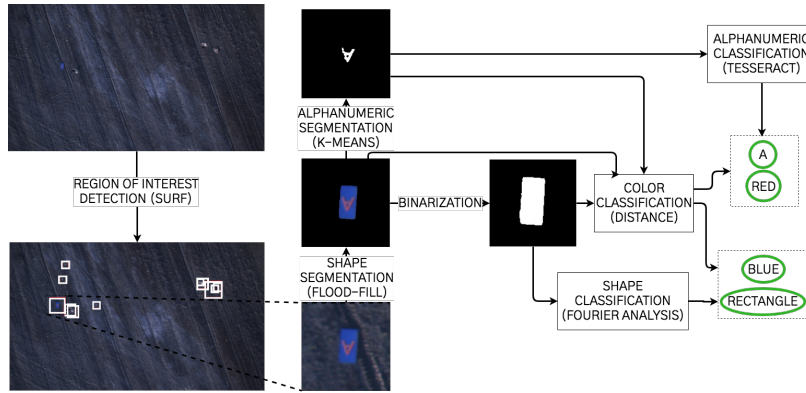


Figure 12: Autonomous Vision System

fails shape and alphanumeric segmentation. If either the shape or alphanumeric returns a low confidence value, the object is not reported. Objects are also filtered if the color of the alphanumeric and shape are classified as the same. The AVS provides the ability to add geofences around the search area and separate out locations where objects are known to not be located (e.g. forests, tent areas, etc.). These areas are marked before takeoff and the system uses the geofences during the mission to filter any targets reported within these regions.

Autonomous Region Merging

During the mission, the object sightings classified by the Autonomous Vision System are sent to the IGS, where they are localized and stored in a database. At the end of the mission, all objects sightings are sent to the AVS, which merges similar sightings into a single object based on location. Merged objects are given higher confidence values if they have similar characteristics. Objects above a certain confidence threshold are reported. Should two sightings be significantly close together and classified as differing shapes or alphanumeric characters, a voting algorithm is applied, where confidence values determine the weights of the votes for each classification criteria. Autonomy is improved by merging object sightings this way to avoid reporting extra objects or false positives.

Tests were conducted on approximately 6000 images taken from test flights, previous competitions, and synthetically generated datasets. These images contain approximately 300 objects, which were manually tagged and used for testing purposes. All object shapes, alphanumerics, and colors are represented.

The statistics in **Table 7** indicate that the system can locate approximately 92% of all objects, and that of all regions of interest, 39% are actual objects. On actual objects, the system performs well at identifying shape, alphanumeric and orientation characteristics.

The complete Autonomous Vision System is dia-

grammed in **Figure 12**.

ROI Precision	39%
ROI Recall	92%
ROI False Positive Rate	4 : 1
Alphanumeric Accuracy	66%
Shape Accuracy	80%
Shape Color Accuracy	70%
Alphanumeric Color Accuracy	45%
Orientation Accuracy	66%

Table 7: Autonomous Vision System Statistics

2.6. Communications

The UAS has three wireless links between the aircraft and the ground station as diagrammed in **Figure 13**. These three links are a 433 MHz spread-spectrum UHF link, a 5GHz WiFi AC link, and a 900 MHz autopilot telemetry link. The UHF link, established using an EzUHF RC radio module acts as the backup RC link. This allows for manual control of the aircraft from the ground. The WiFi link, established by a Ubiquiti Rocket AC pair, provides the main data path between the aircraft and the IGS. The 900 MHz telemetry link, established by a RFD900+ pair, provides a backup for the autopilot ground station. Each link has a set of carefully selected antennae to ensure a reliable connection between the aircraft and the ground station. Additionally, the team uses a NETGEAR R6700 wireless router, operating within the 2.4 GHz frequency band, for communication between systems on the ground.

The wings of the aircraft contain two 2.2 dBi skew-planar wheel antennae attached to the Ubiquiti Rocket AC. The team chose these antennae because of their omnidirectional radiation pattern between 5.65 GHz and 5.95 GHz. This ensures that connectivity is independent of aircraft orientation. The antennae are placed roughly one meter apart to avoid possible interference with the carbon fiber boom and other electronics in the fuselage. An array of two 8 dBi patch antennae are located on

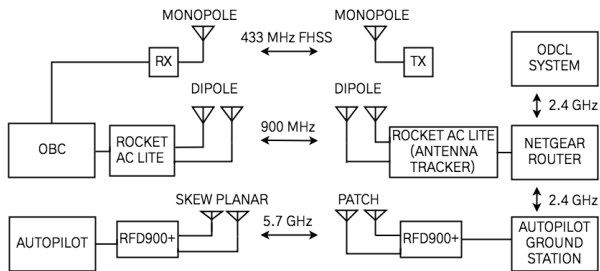


Figure 13: Communications System Diagram

the ground. These antennae are highly directional and improve the system’s link budget and UAS range.

Testing the communications system involves reliability and distance testing the two main wireless links. The WiFi and telemetry links were both established at roughly 650m apart from each other at two locations on Cornell’s campus with line of sight. A test matrix was constructed with various transmission powers and antenna arrays used at both ends of the link. RSSI and data rates were collected over a period of one minute and averaged for each point in the matrix.

The data collected, plotted for the RFD900s in **Figure 14**, allowed the team to not only establish the best performing setup (determined by the highest data rate) but also the most reliable (determined by highest receive power). It was determined from these tests that a $1/2\lambda$ dipole antenna setup on the aircraft maximizes signal strength during flight.

2.6.1. Antenna Tracker

The team built an antenna tracker to orient the patch antenna array towards the aircraft at all times, ensuring no loss in WiFi connectivity. The antenna tracker receives the aircraft’s GPS location from the Autopilot GCS and its own location from an onboard GPS. The vector between the aircraft and antenna tracker is used to calculate the angles required to orient the antennas. These angles are achieved by driving two DC motors responsible for the azimuth and elevation rotation.

The team is confident that the communication system will be reliable enough to achieve the Telemetry Prerequisite for Obstacle Avoidance and provide enough bandwidth between the aircraft and the IGS to achieve Actionable Intelligence.

²John R. Taylor. *Classical Mechanics*. University Science Books, 2005.

³Ibid.

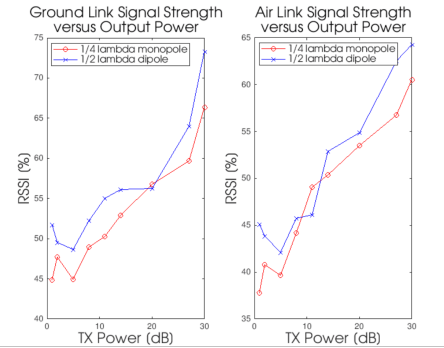


Figure 14: RFD900 Distance Test Results

2.7. Air Delivery

The air delivery system is made up of two primary components, a mechanism that releases the payload and software to determine the optimal release time. Theia II’s delivery mechanism was designed to reduce points of failure and improve drop reliability. The system secures the bottle with a plastic and 3D printed harness that is suspended by the pin of a linear actuator. When signaled, the linear actuator pulls the pin, immediately releasing the payload. The weight of the bottle presses open a flap in the skin and the bottle falls to the ground. Elastic bands retract the flap to reduce aerodynamic disruption. The inside of the air delivery mechanism is insulated from other parts of the fuselage with Garolite to weather proof it from dirt and snow. The team found through drop tests that no additional modifications to the water bottle were necessary to ensure the bottle fractured and dispersed water on impact with pavement or grass at an altitude of 100 feet. The air delivery mechanism is shown in **Figure 15** and **Figure 16**.

Using input from the autopilot, the onboard computer autonomously determines the optimal time to release the bottle. The system first calculates the horizontal distance the bottle will travel by modeling drag. The team chose to approximate the bottle as a sphere with a diameter of 9 cm, the average diameter of the water bottle. Drag on a sphere in free fall can be determined using **Equation 2**, which describes the drag on a sphere in free fall.²

$$m\vec{a} = -m\vec{g} - \beta D\vec{v} - \gamma D^2 v^2 \hat{v} \quad (2)$$

D is the diameter of the sphere and β and γ are linear and quadratic drag constants of a sphere in free fall, respectively. For the 9 cm sphere falling through air, $\beta = 3.3 \times 10^{-6}$ lbfs/ft² and $\gamma = 5.2 \times 10^{-3}$ lbfs²/ft² [3].

Due to the linked dependence between the velocity terms in the quadratic equations, the quadratic drag



term equations can only be solved numerically. The team used MATLAB simulations to create a look-up table for the quadratic drag model that maps the conjunction of airspeed, ground speed, and altitude to a resulting horizontal distance the bottle will travel. The system then releases the bottle when the aircraft is the correct distance away from the target drop location.

To test the air delivery system, the team employed a combination of ground testing and flight testing. The team first tested the structural integrity of the hardware mechanism in the lab by dropping the mechanism from a height of 10 ft onto concrete. The mechanism did not break after 10 drops and the team concluded the mechanism was sturdy enough to support belly landings.

The team used stationary drop tests to measure the reliability of the air delivery system and ensure the bottle always disbursed water on impact. Bottles were dropped in a stairwell from 100 ft, the minimum possible flight altitude. 20 test drops were conducted. The system actuated and released the bottle 100% of the time. The bottle dispersed water 100% of the time.

The team used flight testing to measure and tune the accuracy of the air delivery system. The results of these tests are displayed in **Table 9**.

Mean Drop Accuracy	15 feet
SD of Drop Accuracy	5 feet

Table 9: Summary of test drops of the air delivery system from flight. Note that SD stands for standard deviation. 15 drops were conducted. All drops were from an altitude between 115ft and 130ft.

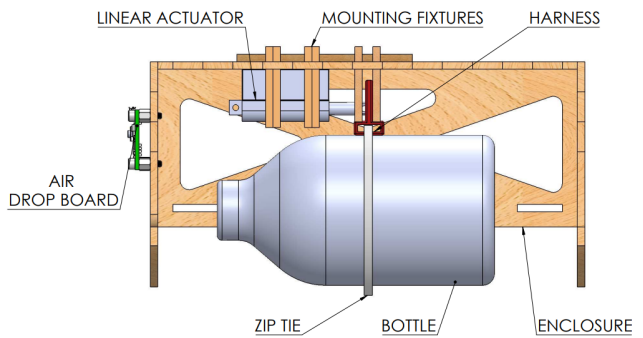


Figure 15: Air Delivery Mechanism, Sideview

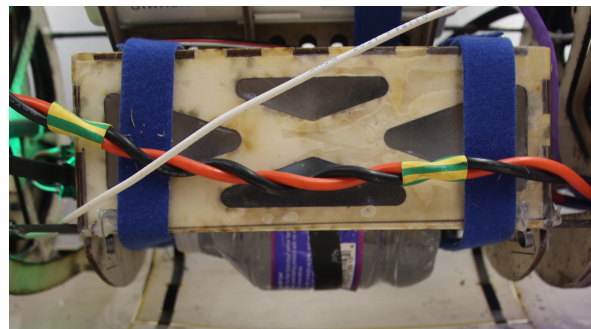
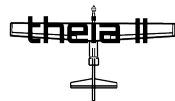


Figure 16: Air Delivery Mechanism

Network		Systems	
RFD900 Radio	<ul style="list-style-type: none"> Protected by AES, the NIST-recommended symmetric encryption protocol FHSS prevents interference from nearby signals on similar frequencies As a fallback, all capabilities of the radios are duplicated by the WiFi system 	GPS	<ul style="list-style-type: none"> The Pixhawk GNSS GPS is resilient to GPS spoofing and jamming due to hardware built directly into the GPS. The module tracks incoming GPS data for inconsistencies to detect spoofing attacks
WiFi	<ul style="list-style-type: none"> Protected by WPA-2, NIST recommended encryption Using a 128-bit key for AES encryption, the network is effectively protected from wireless sniffing 	APIs	<ul style="list-style-type: none"> Write access to API endpoints is restricted to users with authentication The WiFi network is encrypted, protecting confidentiality and integrity
433MHz RC Transmitter	<ul style="list-style-type: none"> Frequency hopping prevents intentional jamming or accidental interference 	On-Board Computer	<ul style="list-style-type: none"> Log-in password protect the on board computer in case the aircraft is intercepted

Table 8: Cyber Attack Mitigation Techniques



2.8. Cyber Security

The team takes a comprehensive approach to ensuring that the Theia II system thwarts cyber attacks whenever possible. In particular, the system is designed to meet three main security goals.

1. Ensure the aircraft only responds to control signals from authorized users such as the GCS or the safety pilot.
2. Maintain the confidentiality of data collected by the aircraft.
3. Maximize the availability of the connection between the aircraft and the ground.

The Theia II system implements several layers of defense to meet these goals. First, because the wireless networks used by the UAS are the most available to an attacker, the team takes extra measures to protect these networks. The “Network” column of **Table 8** describes the use of various protocols to prevent adversaries from eavesdropping or modifying data on the networks and how to limit an adversary’s ability to interfere with the availability of the networks. When possible, all protocols are used according to recommendations of the National Institute of Standards and Technology (NIST), which defines best practices for security protocols in the United States. In addition to securing the network from external threats, the team also employs WPA2 and a WAN firewall to prevent an adversary from gaining direct access to the network. In the unlikely event that an intruder gains access to the network, the team employees access control protocols described further in the “APIs” section of **Table 8**.

Additional security includes an authentication mechanism on the IGS and Autopilot GCS that limits access to critical functions to authorized users and tracks the actions of each system operator. This enables a tiered permission structure. Further, a private key stored on the host machine is used as a key for end-to-end encryption and session signing. The Autopilot GCS requires the operator to enter a password on start up to send actions to the aircraft and all passwords on both systems are independently hashed to prevent password leakage.

3. Safety, Risks, & Mitigation

Safety is fundamental to the development and operation of a UAS. This section describes potential safety risks and details steps taken to mitigate them. Risks are classified by likelihood of occurrence: Rare, Infrequent, and Frequent. Severity is classified by: Low, Medium, High.

3.1. Developmental Risks & Mitigation

As personnel safety is of the utmost importance, numerous safety considerations were made during the development of the system to ensure the safety of team members. CUAir has designated a safety lead to enforce safety protocol and keep relevant medical supplies and safety equipment readily available during development and testing. CUAir has also developed a safety manual that outlines safe operating procedures. All team members are required to read and take a quiz on these procedures. **Table 10** illustrates the three main risks that the team considered during development.

Developmental Risk	Occurrence	Severity	Mitigation
Fabrication Error and Resulting Personnel Injury	Rare	High	<ul style="list-style-type: none"> • Wear Personal Protective Equipment (PPE) including eye protection, closed toed shoes, and protective gloves • Keep lab area and manufacturing area clean • Keep First Aid medical supplies readily accessible
Insufficient personnel training of new team members	Infrequent	High	<ul style="list-style-type: none"> • All personnel must attend safety training seminar • Team members do not use power tools until they are specifically trained to use them
Personal injury due to unit testing hazardous components, such as the motor	Rare	Medium	<ul style="list-style-type: none"> • Unit testing is never performed alone in order to ensure safety • Safety training seminar prepares members to handle possibly dangerous components

Table 10: Summary of Developmental Risk Analysis and Mitigation Strategies



Mission Risk	Occurrence	Severity	Mitigation
Loss of telemetry or RC link to the UAS	Frequent	Medium	<ul style="list-style-type: none"> Preflight range tests Return to Launch (RTL) and aerodynamic termination autopilot failsafes Redundant links over RFD900+ and WiFi
Unexpected throttle ramp-up on ground	Infrequent	High	<ul style="list-style-type: none"> All personnel stand behind horizontal plane of the propeller before throttle is plugged in Plug in throttle from behind aircraft propeller Dual throttle arming necessitates that Theia II is armed both in software and by a physical safety switch
Unexpected Air Delivery release	Infrequent	Medium	<ul style="list-style-type: none"> Air delivery algorithm does not run until the ground station operator gives authorization with the GCS. The operator will only make this authorization when given the requisite clearance from the judges Do not test over populated areas
Autopilot parameter configuration error	Infrequent	Medium	<ul style="list-style-type: none"> Test all surfaces and autopilot sensors before flight Comprehensive checklist to ensure every system is properly examined
Loss of power to flight controller or electrical failure	Rare	High	<ul style="list-style-type: none"> Check battery levels and all connections before flight Use locking connectors whenever possible Redundant power supply to autopilot through BEC to servo rail and through power module
Damage to LiPo batteries	Rare	High	<ul style="list-style-type: none"> Monitored charging Fireproof cases for LiPo transportation Class D fire extinguisher and protocol for crashes and disposal in event of crash
Catapult Failure	Rare	High	<ul style="list-style-type: none"> Strict catapult protocol and training Safety pin prevents unexpected launches
Pilot Error	Rare	High	<ul style="list-style-type: none"> Only fly in weather conditions deemed safe by the pilot No talking right before take-off or during flight to avoid distracting the pilot

Table 11: Summary of Mission Risk Analysis and Mitigation Strategies

3.2. Mission Risks & Mitigation

CUAir has completed a comprehensive analysis of potential safety risks during mission testing and has taken a number of steps to mitigate them. The team determined these risks through test flights, ground tests, and general knowledge of the dangers of air systems technology. **Table 11** describes the risks and their respective mitigation steps that the team considered.

CUAir has further developed a safety checklist that is consulted before every flight to verify that all autopilot, electrical, and mechanical components are adequately secured and functional. Moreover, all test flight personnel must stand behind the line of the propeller and at

least 30 feet away from the aircraft before the throttle is armed. The pilot then gives the pneumatic catapult operator verbal confirmation of the team's preparedness before the aircraft is launched. This procedure is followed during all usages of the Theia II system.

4. Conclusion

During the past year, CUAir dedicated itself to designing, building, and testing the Theia II UAS in preparation for the AUVSI SUAS 2018 mission. Extensive testing was performed on the entire system to ensure that the UAS meets all competition specifications and will perform safely and effectively in the mission.